TÜBİTAK

Turkish Journal of Chemistry

http://journals.tubitak.gov.tr/chem/

Research Article

Turk J Chem
(2018) 42: 639 – 651
© TÜBİTAK
doi:10.3906/kim-1706-45

Schiff base of isoniazid and ketoprofen: synthesis, X-ray crystallographic, spectroscopic, antioxidant, and computational studies

Naima REHMAN[1], Muhammad KHALID[2,3], Moazzam Hussain BHATTI[1,*], Uzma YUNUS[1], Ataualpa Albert Carmo BRAGA[2], Faiz AHMED[2,4], Syed Muddassir ALI MASHHADI[1], Muhammad Nawaz TAHIR[5]

[1]Department of Chemistry, Allama Iqbal Open University, Islamabad, Pakistan
[2]Department of Fundamental Chemistry, Institute of Chemistry, University of São Paulo, São Paulo, Brazil
[3]Department of Chemistry, Khwaja Fareed University of Engineering & Information Technology, Rahim Yaar Khan, Punjab, Pakistan
[4]University Community College, Government College University Faisalabad, Faisalabad, Pakistan
[5]Department of Physics, University of Sargodha, Sargodha, Pakistan

Received: 21.06.2017 • **Accepted/Published Online:** 25.12.2017 • **Final Version:** 01.06.2018

Abstract: Ketoprofen and isoniazid together are a potential combination of a nonsteroidal antiinflammatory drug and an antitubercular medicine to treat tuberculosis and associated symptoms like fever and fatigue. The Schiff base of isoniazid with ketoprofen is synthesized in this research. Infrared spectroscopy (IR) and X-ray diffraction (XRD) analysis of the crystal packing proved the formation of the Schiff base and the existence of N-H$\cdots$O hydrogen bonds between the hydrogen-bonded dimer of the Schiff base. The complete geometrical optimization of the monomer and hydrogen-bonded dimer of the Schiff base is performed utilizing M06-2X/6-31G(d,p) level theory and compared with the experimental data to optimize the molecular structure. The effect of 2,2-diphenyl-1-picrylhydrazyl (DPPH) radical scavenging activity shows that the synthesized Schiff base has improved antioxidant activity. Molecular docking studies against *Mycobacterium tuberculosis* (*Mtb*) RNA polymerase-related targets with PDB codes 2M6O and 4KBJ and lung surfactant protein A (SP-A) with PDB ID 5FFT suggest that it can be screened as a potent drug against *Mtb* infection of the lungs. Frontier orbital theory analysis shows a high energy gap between the HOMO and LUMO, which suggests that the reported Schiff base might be a bioactive compound. Different experimental (XRD, IR, thermal gravimetric analysis, differential scanning calorimetry) and computational studies correlate and validate findings related to this novel Schiff base.

Key words: Isoniazid and ketoprofen Schiff base, X-ray diffraction, density functional theory studies, molecular docking, free radical scavenging activity

1. Introduction

Isoniazid is an efficient drug used in 'triple therapy' against *Mycobacterium tuberculosis* (*Mtb*) since 1952. It is used alone or in combination with other drugs to cure tuberculosis (TB). In tuberculosis and similar diseases, tissue inflammation and free radical eruption from macrophages result in oxidative stress. Pulmonary inflammation occurs if the TB drugs are not used along with antioxidants.[1−3] Furthermore, oxidation reaction results in degradation of the drugs, reducing their shelf life as well as their concentration in blood.

The incorporation of ketoprofen and isoniazid as codrugs might have potent activity in the combination of

*Correspondence: moazzamhussain_b@yahoo.com

a nonsteroidal antiinflammatory drug (NSAID) and an antiinfective medicine. Ketoprofen (2-(3-benzoylphenyl)-propionic acid) is a famous NSAID. It exhibits antiinflammatory, antipyretic, and analgesic properties.[4] It also acts as a prostaglandin synthetase inhibitor.[5] It has also been used to reduce fever.[6] Ketoprofen causes gastrointestinal tract disturbances,[7] which restricts its use in local and parenteral applications.[8] Several techniques have been established to enhance the efficacy of the drug using addition of surface active agents, formation of water-soluble salts, or polymers to increase the bioavailability of the drug.[9–11] A systematic study of molecular crystals as well as codrug formation strategy would offer diverse options for drug modulation of such a chemically labile drug.[12–15]

The Schiff base of isoniazid and ketoprofen may be used to treat TB as well as fever and fatigue related to tuberculosis. Schiff bases have medicinal and pharmaceutical importance due to a broad range of biological activities like antiinflammatory,[16] antimicrobial,[17–19] antioxidant, and antitubercular activities.[20–29] The heterocyclic systems having azomethine functionality in Schiff bases are known to possess cytotoxic, antimicrobial, anticancer, and antifungal activities.[30–33] The chemical reaction for the synthesis of the Schiff base is shown in the Scheme.

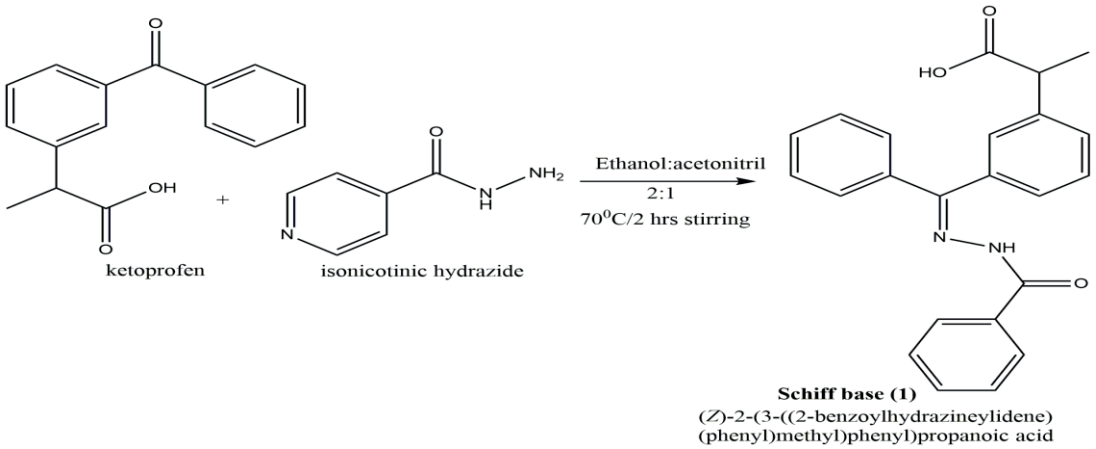

Scheme. Chemical reactions for synthesis of the Schiff base.

2. Results and discussion

2.1. X-ray crystallographic study

Single-crystal X-ray diffractions revealed the formation of the Schiff base of ketoprofen with isoniazid (Figure 1a), which dimerizes with another molecule of the Schiff base (Figure 1b). Crystal information data are summarized in Table 1. In this compound, there is an imine bond, which is also confirmed by bond lengths C10-N1 = 1.284 Å and N1-N2 = 1.382 Å, respectively. Similarly, the two carbonyl C=O groups also exist in the compound with bond lengths of C1-O1 = 1.295 Å and C1-O2 = 1.1893 Å. Strong classical intramolecular hydrogen bonding motifs also exist for the novel dimeric compound O1-H1–N3 [O1-H1 = 0.82 Å, O1–N3 = 2.6983 Å, O1-H1–N3 = 173.8°], as given in Table 2. The packing structure with cell axes is shown in Figure 1c.

The crystal structure has been deposited at the Cambridge Crystallographic Data Centre and its assigned CCDC number is 1416575.

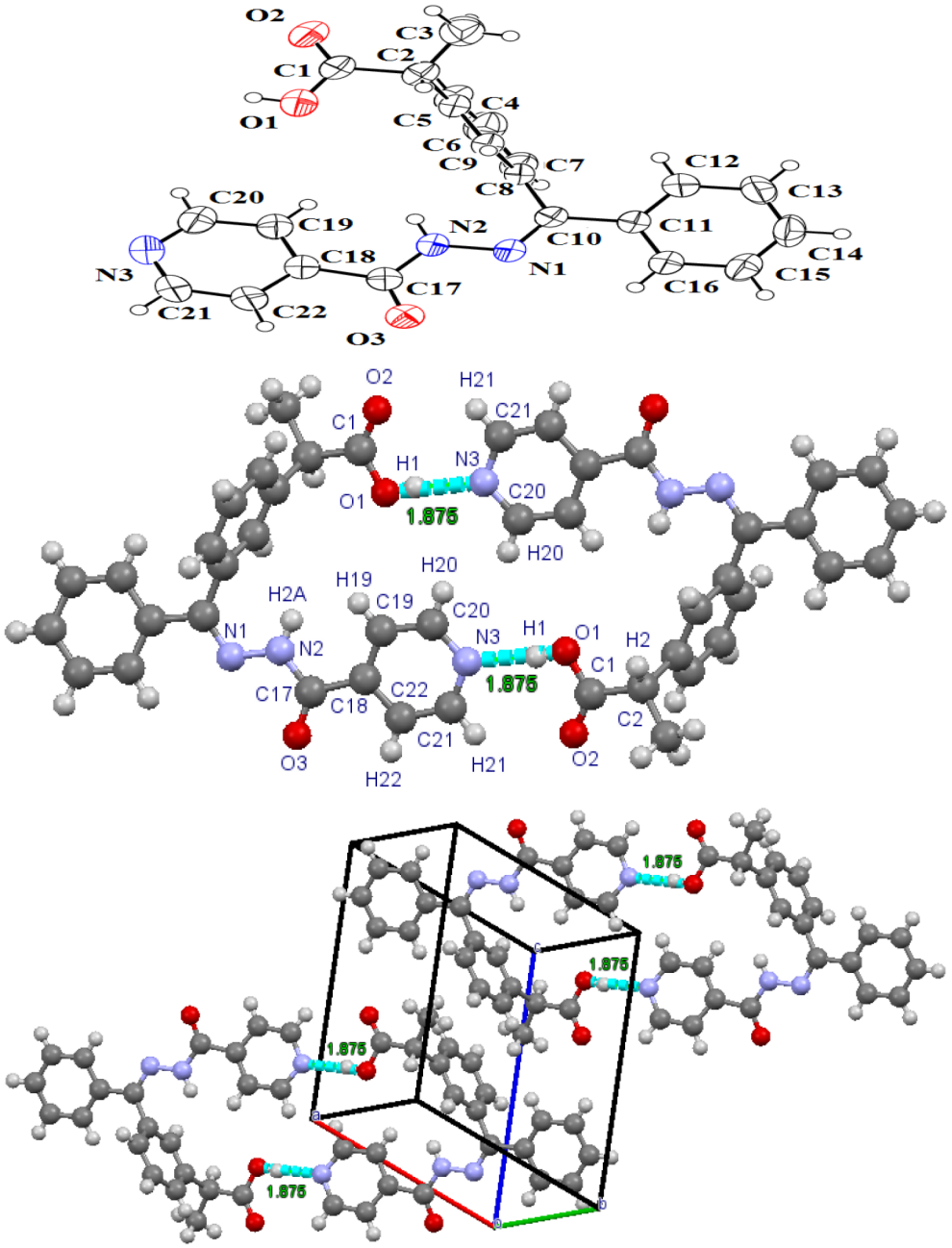

Figure 1. a. Structure of the Schiff base showing the atom-labeling scheme. Displacement ellipsoids are drawn at the 50% probability level. b. Hydrogen-bonded dimer of the Schiff base. c. The packing structure with cell axes.

2.2. FT-IR analysis

The FT-IR spectrum of the Schiff base showed vibrational band of N-H at 3355 cm^{-1}. There were two stretching vibrations bands of C=O at 1713 cm^{-1} and 1697 cm^{-1}, which confirmed the presence of the carbonyl group of carboxylic acid and a carbonyl group of the amide functional group, respectively. A C=N stretching vibration band was observed at 1657 cm^{-1}, which identified the formation of the Schiff base of ketoprofen and isoniazid.

Table 1. Single-crystal XRD data of the Schiff base.

Compound	Crystal data
Chemical formula	$C_{22}H_{19}N_3O_3$
M_r	373.40
Crystal system, space group	Triclinic, $P1$
Temperature (K)	296
a, b, c (Å)	9.1920 (4), 10.5431 (4), 11.1652 (5)
α, β, γ (°)	74.516 (2), 65.855 (2), 84.240 (3)
V (Å^3)	951.49 (7)
Z	2
Radiation type	Mo $K\alpha$
μ (mm^{-1})	0.09
Crystal size (mm)	0.36 × 0.30 × 0.26
Data collection	
Diffractometer	Bruker Kappa APEXII CCD
Absorption correction	Multiscan (*SADABS*; Bruker, 2005)
T_{min}, T_{max}	0.970, 0.978
No. of measured, independent, and observed $[I > \sigma(I)]$ reflections	14098, 3692, 2457
R_{int}	0.029
sin $theta/\lambda_{\max}$ (Å^{-1})	0.617
Refinement	
$R[F^2 > 2\sigma\ (F^2)]$, $wR(F^2)$, S	0.058, 0.174, 1.04
No. of reflections	3692
No. of parameters	256
H-atom treatment	H-atom parameters constrained
$\Delta\rangle_{\max}$, $\Delta\rangle_{\min}$ (e Å^{-3})	0.51, –0.24

Computer programs: APEX2 (Bruker, 2007), SAINT (Bruker, 2007), SHELXS97 (Sheldrick, 2008), SHELXL2014/6 (Sheldrick, 2015), ORTEP-3 for Windows (Farrugia, 1997), PLATON (Spek, 2009), WinGX (Farrugia, 1999).

Table 2. Hydrogen bond distance and angles in the Schiff base.

Atoms	D—H (Å)	H–A (Å)	D–A (Å)	D—H—A (°)
O(1)-H(1)–N(3)	0.82	1.88	2.69 (3)	173.80

Moreover, stretching vibrations of medium intensity at 1325 cm^{-1} and 1226 cm^{-1} also identified the presence of C-N and C-O functional groups, respectively. The spectrum is shown in the Supplementary Information (Figure S2).

2.3. DSC measurements

The DSC measurements showed that the Schiff base exhibited an endothermic peak at 235.53 °C (Figures S3 and S4 in the Supplementary Information). Complete information regarding this experiment is provided in Table S1 (Supplementary Information).

2.4. Free radical scavenging activity

The free radical scavenging activity was studied using the DPPH model system.[34] Similarly, the IC_{50} value was also calculated. The DPPH test demonstrated the activity of the Schiff base with stable free radicals and its effect is due to its hydrogen donating capacity. A higher IC_{50} value signifies decreased antioxidant activity and vice versa. The Schiff base displayed higher radical scavenging activity with an IC_{50} value of 6.12 ppm than that of ketoprofen and isoniazid (Figure S5 and Table S3, Supplementary Information).

2.5. Computational studies

The optimized geometric parameters of the Schiff base are listed in Table S4 of the Supplementary Information. They are compared with experimentally determined parameters. The comparative study shows that the calculated bond lengths are slightly greater than the experimentally determined bond lengths; see Table S5 (Supplementary Information). This is expected because the experimental data belong to the solid phase while the density functional theory (DFT) calculations correspond to the gaseous phase. The theoretical bond angles of the Schiff base are also investigated in the current study, as can be seen in Table S4 (Supplementary Information). A close difference is found between theoretically and experimentally determined bond lengths and bond angles. Deviation in the selected bond lengths and bond angles of the title molecule is observed in the range of 0.047 $\pm$ 0.023 Å and 2.3 $\pm$ 1.9°, respectively. The maximum deviation in the bond length 0.047 Å is observed for C(2)-C(3) while 2.3° deviation in the bond angle is found in C(1)-C(2)-C(3). The bond length between carbon and oxygen atoms calculated through DFT is found to be 1.326 and 1.213 Å for C(1)-O(26) and C(1)-O(27), respectively, while XRD calculated the same to be 1.305 and 1.199 Å, respectively. Divergence in bond length of C(10)-N(23), C(17)-N(24), C(20)-N(25), C(21)-N(25), and N(23)-N(24) is observed as 1.288, 1.369, 1.336, 1.34, and 1.358 Å through DFT and 1.284, 1.348, 1.326, 1.325, and 1.381 Å through XRD, respectively. The calculated bond angles tabulated in Table S4 (Supplementary Information) between O(26)-C(1)-O(27) and C(10)-N(23)-N(24) are observed as 124° and 116.1° (DFT) and as 122.9° and 116° (EXP), respectively.

2.5.1. Natural bond orbital analysis

We have concluded that the dimer of the Schiff base has hydrogen bonding as shown in Figure 1b and this dimer consists of two N$\cdots$H-O hydrogen bonds with equal distance. To explain the driving force in the formation of the H-bond strengthening in the dimer of the Schiff base, natural bond orbital (NBO) analysis was carried out for the H-bond and all other types of interactions existing in the dimer structure, as shown in Figure 2.

In the NBO study, the H-bond in the dimer of the Schiff base was associated with an intermolecular donor–acceptor interaction where the lone pair orbital of the nitrogen atom in the pyridine ring delocalizes into the antibonding orbitals HO* of the carboxylic functional group (HO-C=O) of the other monomer. The stabilization energy because of the donor–acceptor interaction can be characterized using second-order perturbation theory in the NBO analysis.[35–39]

NBO (i) represents the donor, NBO (j) represents the acceptor, and $E^{(2)}$ means stabilization energy corresponding to the delocalization of electrons between the donor and acceptor with a relationship as follows:

$$E^{(2)} = q_i \times (((F_{i,j})^2)/(\varepsilon_j - \varepsilon_i)) \quad (1)$$

Here q_i, ε_i, ε_j, and $F_{i,j}$ represent orbital occupancy, diagonal, off-diagonal, and NBO Fock matrix elements, respectively.

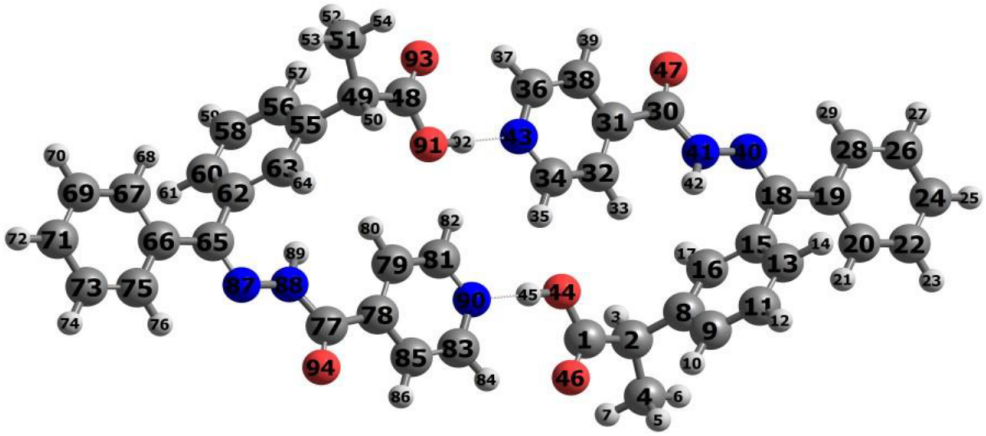

Figure 2. The optimized geometry of the Schiff base dimer by applying M06-2X/6-31G(d,p) method showing hydrogen bond and atom labels.

NBO analysis showed donor–acceptor interactions in the hydrogen bonding of the dimer Schiff base structure. This is because of the delocalization of the lone pair orbitals (nN) of N43 LP and N90 LP to the antibonding orbitals (σ*) of O91-H92 and O44-H45. In both cases the second-order stabilization energy is found to be 17.72 kJ mol^{-1}, as can be seen in Table S5 (Supplementary Information).

The obtained stabilization energy suggests that the hydrogen bonds in the dimer Schiff base have equal strengthening, which is in good agreement with the experimentally determined structure.

Moreover, additional donor–acceptor interactions found are the reason for stability in the dimer of the Schiff base and the stabilization energies have been determined to be 3.63, 3.15, 2.75, 4.36, and 2.61 kJ mol^{-1} because of the σ(C1-C2) $\rightarrow$ σ * (O44 -H45), σ(C2-H3) $\rightarrow$ σ * (C1-O46), σ(C15-C18) $\rightarrow$ σ * (C11-C13), σ(C16-H17) $\rightarrow$ σ * (C8–C9), and σ(C18-H19) $\rightarrow$ σ * (C19-C28), respectively. Interestingly, the NBO study also exhibits stronger stabilizing $Q \rightarrow Q*$ interactions in our title dimer, Q (C8-C9) $\rightarrow$ $Q*$(C11-C13) and Q*(C15-C16), Q (C11-C13) $\rightarrow$ $Q*$(C8-C9) and Q*(C15-C16), and Q (C15-C16) $\rightarrow$ $Q*$(C8-C9) and Q*(C11-C13) consisting of 29.66, 29.84, 27.68, 32.67, 29.11, and 27.82 kJ mol^{-1}, respectively. These stabilization energies have been described here just as a model in order to show $Q \rightarrow Q*$ interactions, and many $Q \rightarrow Q$* stabilization energies have been found in this system as shown in Table S5. These energies suggest that the $Q \rightarrow Q*$ interactions provide stronger stabilization to the structure. Some interactions corresponding to the resonance in the dimer also exist as donation of electrons from a lone pair (LP) of atoms to σ* and Q*, showing strong stabilization energy with magnitude reaching up to 77.66 kJ mol^{-1} and 70.04 kJ mol^{-1} in our system, as shown in Tables S5 and S6, respectively (Supplementary Information).

Based on the NBO study, we can conclude that the strong intramolecular hyperconjugation interactions and intermolecular hydrogen bonding are responsible for the more stable dimer conformation in the gas and solvent phases, which also exist in the solid-state structure.

2.5.2. Molecular electrostatic potential

The electron density map with standard electrostatic potential colors for the dimer of the Schiff base shows the electron density at different places on the dimer (Figure 3). The red color in the electron density map indicates the electron-rich places as oxygen and nitrogen atoms and the blue color represents the electron-deficient region

as hydrogen atoms. As per the map, the area around the oxygen and nitrogen atoms is strongly negative, whereas all the H atoms in the dimer are positive.

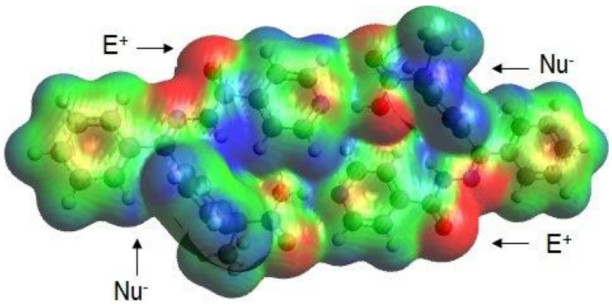

Figure 3. The electron density map of the dimer of the Schiff base determined by M06-2X/6-31G(d,p) method.

2.5.3. Thermochemistry

Thermodynamic parameters have been retrieved via the usage of a frequency calculation in Gaussian 09. The enthalpy change (ΔH) and energy change (ΔG) are calculated to be –288.7 and –125.5 kcal/mol, respectively, Eqs. (2) and (3). The results suggest that the dimer is energetically favorable in comparison to monomers, probably due to the hydrogen bonds.

$$\Delta H = H_{dimer} - 2 \times H_{monomer} \tag{2}$$

$$\Delta G = G_{dimer} - 2 \times G_{monomer} \tag{3}$$

2.5.4. Frontier orbital energy analysis

The study of the frontier orbital energy theory leads to valuable information with respect to the biological mechanism. As per this theory,s the energy gap between HOMO and LUMO is the most critical element that controls the bioactivity. The energy of HOMO and LUMO and their energy gap are calculated employing DFT in THF solvent and results are presented in Table S7 (Supplementary Information).

The HOMO and LUMO energy gap in the Schiff base is found to be 0.2330 a.u., while the energy gap between HOMO-1 and LUMO+1 is 0.2331 a.u. (Figure 4).

The energies of FMOs are helpful to determine the global reactivity descriptors, which are calculated using equations given in the Supplementary Information, and results are arranged in Table S7. Results from Table S7 reveal that the global softness (S) value of the Schiff base is 4.2902 E_h, which is 38 times greater than its global hardness (η) 0.1119 E_h value. This greater softness value is because of a low HOMO–LUMO energy gap. These findings of low energy gap and greater softness value suggest that the Schiff base might be bioactive.[40–43]

2.6. Molecular docking

Transcription initiation and transcription activators play a critical role in the highly regulated process of gene expression. RbpA is an essential small non-DNA-binding transcription factor associated with RNA polymerase holoenzyme and stimulates transcription in actinobacterial *Mtb*.[44] In *Mtb*, the gene product of *Rv3583c* is essential for its survival, marked as CarD, and it has been identified as an essential protein in vitro and in vivo

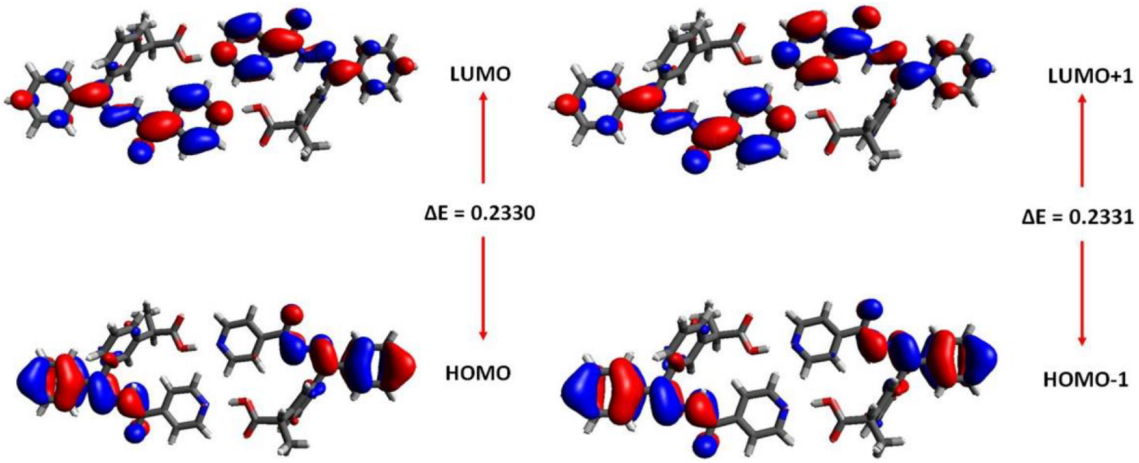

Figure 4. HOMO and LUMO energy gap.

during normal as well as genotoxic stress and in nutrient deprivation environments.[45] The RNA polymerase (RNAP) β-subunits are structurally vastly preserved among different kingdoms of living organisms, even though conservation of the sequence is low. During transcription, bacterial RNAP $\beta 1$ and $\beta 2$ domains are involved in various processes, i.e. downstream DNA binding and selection of the transcription initiation site, formation and stabilization of the open complex, and maintaining the proper transcription bubble via downstream DNA gripping.[46] Surfactant protein A (SP-A) is a collagenous C-type lectin (collectin) that is critical for pulmonary defense against inhaled microorganisms. The differential binding properties of SP-A favor transfer of the material from surfactant dipalmitoyl phosphatidylcholine (DPPC) to pathogen membranes, DPPC being the major component of surfactant membranes lining the air/liquid interface of the lung, which plays a key role in host defense functions.[47]

In docking studies, we tried to identify the interaction of our synthesized Schiff base with *Mtb* RNAP, *Mtb* RbpA, and SP-A. Docking results show that our Schiff base does not form hydrogen bonds with SP-A. A high kinase inhibition (kI) value of 828.34 μM for this complex, as predicted, will not affect its functionality and it can be easily transported from blood plasma to our target *Mtb* through SP-A. On the other hand, it forms hydrogen bonds with ASP67 and an undefined residue in *Mtb* RbpA (PDB-ID: 2M6O), while in case of Mtb RNAP (PDB-ID: 4KBJ Chain-B) it forms hydrogen bonds with VAL168 and VAL170, as shown in Figures 5a and 5b, respectively. It also forms a stable complex with low kI values and has the ability to alter the proper functionality of these two factors. Thus, the kI values along with calculated energy changes (Table 4) for the most stable conformation (Figures 5c–5f) support our idea that it might be used as a potent drug against *Mtb*. For our synthesized Schiff base, the Actelion Pharmaceuticals Ltd. Osiris Property Explorer calculations cLogP = 3.31, cLogS = –5.05, and drug likeliness = 3.95 with overall drug score = 0.22 reinforce that it will be more effective against *Mtb* with fewer side effects as compared to isoniazid, which has a drug score of 0.06.

2.7. Conclusion

The Schiff base of ketoprofen with isoniazid has been synthesized in crystalline form and characterized by FT-IR, X-ray crystallographic, DSC, and computational studies. The DPPH radical scavenging (antioxidant) studies revealed that the Schiff base has a lower IC_{50} value, signifying its high antioxidant activity. Docking studies along with OSIRIS calculations and good agreement with Lipinski's rule also reinforce our thought

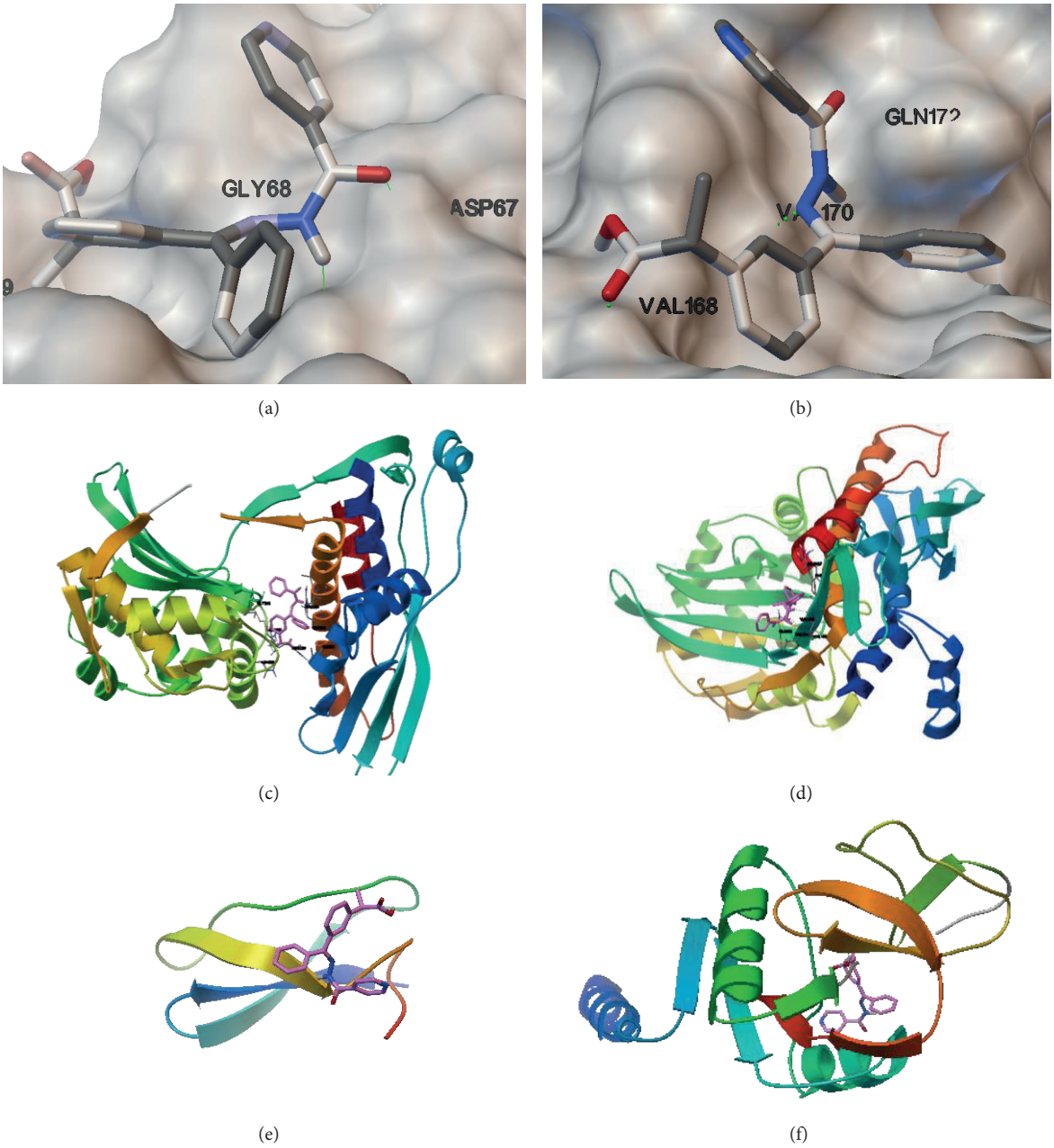

Figure 5. a–f) Docking conformation of ligand with *Mtb* RNAP, RbpA, and SP-A.

that it would be more potent against *Mtb* infection as compared to isoniazid. DFT analysis at the M06-2x levels with the 6-31G(d,p) basis set and its comparison with experimental results shows a reasonably good agreement between them. NBO study reconfirmed the N$\cdots$H-O hydrogen bonds between the monomers of the Schiff base. The enthalpy change (ΔH) data suggest that the dimer is energetically favorable in comparison to monomers, probably due to the hydrogen bonds. Moreover, the strong intramolecular hyperconjugative interactions responsible for the more stable dimer conformation in the gas phase suggested by the NBO study are also present in the solid-state structure. The frontier molecular orbital energies gap of the title compound

Table 3. IR spectral data of the Schiff base.

Functional groups	(ν cm^{-1})
Asymmetric-NH_2 stretching	3355
Aromatic C-H stretching	3010
C=O stretching	1713, 1697
C=N stretching	1657
Aromatic ring vibrations	1606, 1483
C-N stretching	1325
C-O stretching	1226

Table 4. Molecular docking details of stable ligand receptor complex.

Figure no.	Receptor PDB ID	Binding energy	kI, μM	Intermolecular energy	Internal energy	Ligand torsional energy
5c	4KBJ chain-A	–5.57	83.07	–7.65	–1.77	2.09
5d	4KBJ chain-B	–6.04	37.41	–8.13	–1.83	2.09
5e	2M6O	–5.94	44.22	–8.03	–1.79	2.09
5f	5FFT	–4.2	828.34	–6.29	–1.78	2.09

was determined at 6.298 eV between the HOMO and LUMO, suggesting that the Schiff base might be bioactive, which shows good agreement with the antioxidant and docking studies.

3. Experimental

3.1. Materials and methods

All reagents were used as purchased without further purification from the suppliers. Solvents were dry-distilled in accordance with standard protocols before use. Melting point determination was carried out using an electrothermal apparatus made by Gallenkamp (UK) with specifications of 50 Hz, 220/240 V. The result was consistent with the results of DSC. The DSC experiment was carried out with a Mettler Toledo instrument. At 10 °C/min with nitrogen flow, samples (2–5 mg) were heated in open aluminum pans.

The IR spectrum was recorded using a Varian 640-IR spectrophotometer in ATR mode. X-ray data were obtained using a Bruker Kappa APEX II CCD diffractometer equipped with a graphite monochromator at 296 K. Clear resolution of the molybdenum Kα tube was used. Data collection was done using APEX2 software and SAINT for the number of refection indices and determining the unit cell parameters. The molecular structures along with geometrical parameters such as bond distances and bond angles could be solved by SHELXS-97. Mercury 3.7 software was used to generate the figures and to perform other calculations. Antioxidant studies were carried out spectrophotometrically and a UV-1700 (Shimadzu, Japan) was used for this purpose. Table curve software was used to calculate IC_{50} values of tested compounds.

3.2. Synthesis

Ketoprofen (0.5 g, 0.002 mol) and isoniazid (0.3 g, 0.002 mol) were separately dissolved in 20 mL of a binary mixture of ethanol and acetonitrile (2:1). Both solutions were mixed and stirred for 2 h at about 70 °C and

kept for slow evaporation for several days. Light yellow prism-like crystals having m.p. 235 °C were separated by filtration and dried under normal conditions.

3.3. Free radical scavenging activity

The effect of the DPPH radical as a scavenger was determined as illustrated by Blois with certain variations.[48] A 1 mM DPPH solution (0.1 mL) in methanol was incubated with various concentrations of the Schiff base. After 30 min of incubation at normal temperature, absorbance of the resulting solution was recorded at 514 nm. DPPH radical scavenging activity can be expressed as in Eq. (4).

$$\%Activity = ((Abs_{control} - Abs_{sample})/Abs_{control}) \times 100 \quad (4)$$

In this method, the Schiff base as an antioxidant reacts with the stable DPPH (deep violet color), which converted into 2,2-diphenyl-1-picrylhydrazine with discoloration (Figure S1, Supplementary Information). The extent of discoloration represents the scavenging potential of the antioxidant sample. Gallic acid was used as a standard for comparison.

3.4. Computational procedures

All computational calculations were carried out using the Gaussian 09 software package,[49] based on DFT.[50] Geometry optimization and frequency calculations for the Schiff base were performed and the lack of negative eigenvalues indicates that the result of the geometry optimization was true minima on the global potential energy surface. The NBO, HOMO and LUMO, enthalpy change (ΔH), and energy change (ΔG) were calculated using the M06-2X/6-31G(d,p) method. GaussView 5.0 was used for the preparation of input and analysis of output files.[51]

3.5. Molecular docking

Docking calculations were carried out on *Mycobacterium tuberculosis* RNA polymerase beta subunits B1 and B2 (PDB ID: 4KBJ),[46] actinobacterial transcription factor RbpA (PDB ID: 2M6O),[47] and surfactant protein A (SP-A) (PDB ID: 5FFT). These receptors' files were obtained from the RCSB protein data bank and processed with the help of BIOVIA/Discovery Studio 2016, while ligand structures were optimized using Avogadro software for docking studies.[52] AutoDockTools-1.5.6 (ADT) was used to carry out docking calculations.[53] Nonpolar hydrogen atoms were merged and used a rigid file of the receptor molecule. Gasteiger and Kollman charges were added to the receptor molecule. Affinity (grid) maps of 60 × 60 × 60 Å grid points and 1.00 Å spacing were generated using the AutoGrid program, while for RbpA 0.614 Å spacing was set. ADT default parameters and functions were used in the calculation of the electrostatic, bonding, and energy calculations.

Docking simulations were done using the Lamarckian genetic algorithm (LGA 4.2). Initial position, orientation, and six torsions of the ligand molecules were set and the most stable conformation of the ligand was used with the receptor to evaluate docking analysis.

Acknowledgments

The authors are grateful to Allama Iqbal Open University, Islamabad, Pakistan; Departamento de Química Fundamental, Instituto de Química, Universidade de São Paulo, São Paulo, 05508-000, Brazil; HEC Pakistan; and Dr Ana Paula L Batista for her suggestions, cooperation, and careful reading of the article.

References

1. Kwiatkowska, S.; Piasecka, G.; Zieba, M.; Piotrowski, W.; Nowak, D. *Respir. Med.* **1999**, *93*, 272-276.
2. Walubo, A.; Smith, P. J.; Folb, P. I. *Biomed. Environ. Sci.* **1995**, *8*, 106-113.
3. Strausz, J.; Muller-Quernheim, J.; Steppling, H.; Nagel, M.; Ferlinz, R. *Pub. Med.* **1990**, *44*, 222-223.
4. Charles, M. H.; Simon, J. G.; John, H. *Int. J. Pharm.* **2003**, *261*,165-169.
5. Yalcin, T.; Gulgun, Y.; Umit, G. *Farmaco* **1999**, *54*, 648-652.
6. Jachowicz, R.; Nurnberg, E.; Pieszczek, B. *Int. J. Pharm.* **2000**, *206*, 13-21.
7. Lagrange, F.; Pénhourcq, F.; Matoga, M.; Bannwarth, B. *J. Pharm. Biomed. Anal.* **2000**, *23*, 793-802.
8. Tettey-Amlalo, R. N. O.; Kanfer, I. *J. Pharm. Biomed. Anal.* **2009**, *50*, 580-586.
9. Vergote, G. J.; Vervaet, C.; Driessche, I. V. *Int. J. Pharm.* **2001**, *219*, 81-87.
10. Makiko, F.; Naohide, H.; Kumi, S. *Int. J. Pharm.* **2000**, *20*, 117-125.
11. Schultheiss, N.; Newman, A. *Cryst. Growth Des.* **2009**, *9*, 2950-2967.
12. Jones, W. D. S.; Motherwell, A. V. *MRS Bull.* **2006**, *31*, 875-879.
13. Almarsson, O.; Zaworotko, M. *J. Chem. Commun.* **2004**, *17*, 1889-1896.
14. Mashhadi, S. M. A.; Yunus, U.; Bhatti, M. H.; Tahir, M. N. *J. Mol. Struc.* **2014**, *1076*, 446-452.
15. Mashhadi, S. M. A.; Yunus, U.; Bhatti, M. H.; Ahmad, I.; Tahir, M. N. *J. Mol. Struc.* **2016**, *1117*, 17-21.
16. Sathe, B. S.; Jaychandran, E.; Jagtap, V. A.; Sreenivasa, *Int. J. Pharm. Res. Dev.* **2011**, *3*, 164-169.
17. Sondhi, S. M.; Singh, N.; Kumar, A.; Lozach, O.; Meijer, L. *Bioorg. Med. Chem.* **2006**, *14*, 3758-3765.
18. Pandey, A.; Dewangan, D.; Verma, S.; Mishra, A.; Dubey, R. D. *Int. J. Chem. Tech. Res.* **2011**, *3*, 178-184.
19. Chinnasamy, R. P.; Sundararajan, R.; Govindaraj, S. *J. Adv. Pharm. Tech. Res.* **2010**, *1*, 342-347.
20. Wei, D.; Li, N.; Lu, G.; Yao, K. *Science in China B* **2006**, *49*, 225-229.
21. Sidwell, R. W.; Huffman, J. H.; Khare, G. P.; Allen, L. B.; Witkowski, J. T.; Robins, R. K. *Science* **1972**, *177*, 705-706.
22. Witkowski, J. T.; Robins, R. K.; Khare, G. P.; Sidwell, R. W. *J. Med. Chem.* **1973**, *16*, 935-937.
23. Clemons, M.; Coleman, R. E.; Verma, S. *Cancer Treat. Rev.* **2004,** *30*, 325-332.
24. Budavari, S. *The Merck Index*; Merck: Whitehouse Station, NJ, USA, 1996.
25. Haber, J. *J. Czech Phys.* **2001**, *140*, 596-604.
26. Walczak, K.; Gondela, A.; Suwiński, J. *Eur. J. Med. Chem.* **2004**, *39*, 849-853.
27. Holla, B. S.; Poojary, K. N.; Rao, B. S. *Eur. J. Med. Chem.* **2002**, *37*, 511-517.
28. Holla, B. S.; Veerendra, B.; Shivananda, M. K. *Eur. J. Med. Chem.* **2003**, *38*, 759-767.
29. Amir, M.; Shikha, K. *Eur. J. Med. Chem.* **2004**, *39*, 535-545.
30. Almasirad, A.; Tabatabai, S. A.; Faizi, M. *Bioorg. Med. Chem. Lett.* **2004**, *14*, 6057-6059.
31. Tarafder, M. T. H.; Kasbollah, A.; Saravanan, N. *J. Biochem. Mol. Biol. Biophys.* **2002**, *6*, 85-91.
32. Vicini, P.; Geronikaki, A.; Incerti, M. *Bioorg. Med. Chem.* **2003**, *11*, 4785-4789.
33. Bekircan, O.; Kahveci, B.; Küçük, M. *Turk. J. Chem.* **2006**, *30*, 29-40.
34. Sanner, M. F. *J. Mol. Graphics Mod.* **1999**, *17*, 57-61.
35. Kumar, G. S. S.; Kumaresan, S.; Muthu Prabu, A. A.; Seethalakshmi, P. G. *Spectrochim. Acta A Mol. Biomol. Spectrosc.* **2013**, *A-101*, 244-263.
36. Tahir, M. N.; Khalid, M.; Islam, A.; Mashhadi, S. M. A.; Braga, A. A. C. *J. Mol. Struct.* **2017**, *1127*, 766-776.

37. Naseem, S.; Khalid, M.; Tahir, M. N.; Halim, M. A.; Braga, A. A. C.; Naseer, M. M.; Shafiq, Z. *J. Mol. Struct.* **2017**, *1143*, 235-244.

38. Arshad, M. N.; Al-Dies, A. M.; Asiri, A. M.; Khalid**,** M.; Birinji, A. S.; Al-Amry, K. A.; Braga, A. A. C. *J. Mol. Struct.* **2017**, *1141*, 142-156.

39. Sumrra, S. H.; Mushtaq, F.; Khalid, M.; Raza, M. A.; Nazar, M. F.; Ali, B.; Braga, A. A. C. *Spectrochim. Acta A Mol. Biomol. Spectrosc.* **2018**, *190*, 197-207.

40. Sheela, N. R.; Muthu, S.; Sampathkrishnan, S. *Spectrochim. Acta A Mol. Biomol. Spectrosc.* **2014**, *120*, 237-251.

41. Hoque, M. M.; Halim, M. A.; Rahman, M. M.; Hossain, M. I.; Khan, M. W. *J. Mol. Struct.* **2013**, *1054*, 367-374.

42. Adeel, M.; Braga, A. A. C.; Tahir, M. N.; Haq, F.; Khalid, M.; Halim, M. A. *J. Mol. Struct.* **2017**, *1131*, 136-148.

43. Demircioglu, z.; Albayrak, C.; Buyukgungor. O. *J. Mol. Struct.* **2014**, *1065*, 210-222.

44. Reed, A. E.; Curtiss, L. A.; Weinhold, F. *Chem. Rev.* **1988,** *88*, 899-926.

45. Stallings, C. L.; Stephanou, N. C.; Chu, L.; Hochschild, A.; Nickels, B. E. *Cell* **2009**, *138*, 146-159.

46. Frisch, M. J.; Nielsen, A. B.; Holder, A. J. *GaussView User's Manual*; Gaussian Inc.: Pittsburgh, PA, USA, 2000.

47. Salazar, A. T.; Doughty, B. L. P.; Lewis, R. A.; Ghosh, S.; Parsy, M.; Simpson, P. J.; Dwyer, K. O.; Matthews, S. J.; Paget, M. S. *Nucleic Acids Res.* **2013**, *41*, 5679-5691.

48. Bekircan, O.; Bektas, H. *Molecules* **2008**, *13*, 2126-2135.

49. Kahveci, B.; Bekircan, O.; Karaoglu, Ş. A. *Ind. J. Chem.* **2005**, *44*, 2614-2617.

50. Frisch, M. J.; Trucks, G. W.; Schlegel, H. B.; Scuseria, G. E.; Robb, M. A.; Cheeseman, J. R.; Scalmani, G.; Barone, V.; Mennucci, B.; Petersson, G. A. et al. *Gaussian 09, Revision D.01*; Gaussian, Inc.: Wallingford, CT, USA, 2009.

51. Hohenberg, P.; Kohn, W. *Phys. Rev.* **1964**, *136*, 864-871.

52. Hanwell, M. D.; Curtis, D. E.; Lonie, D. C.; Vandermeersch, T.; Zurek, E.; Hutchison, G. R. *J. Cheminform.* **2012**, *4*, 1-17.

53. Goh, B. C.; Wu, H.; Rynkiewicz, V.; Schulten, K.; Seaton, B. A.; McCormack, F. X. *Biochemistry* **2016**, *55*, 3692-3701.

Supplementary information

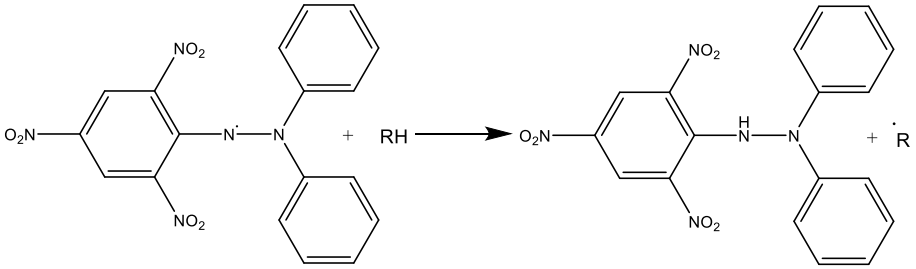

Figure S1. Reaction of antioxidant with stable DPPH free radical.

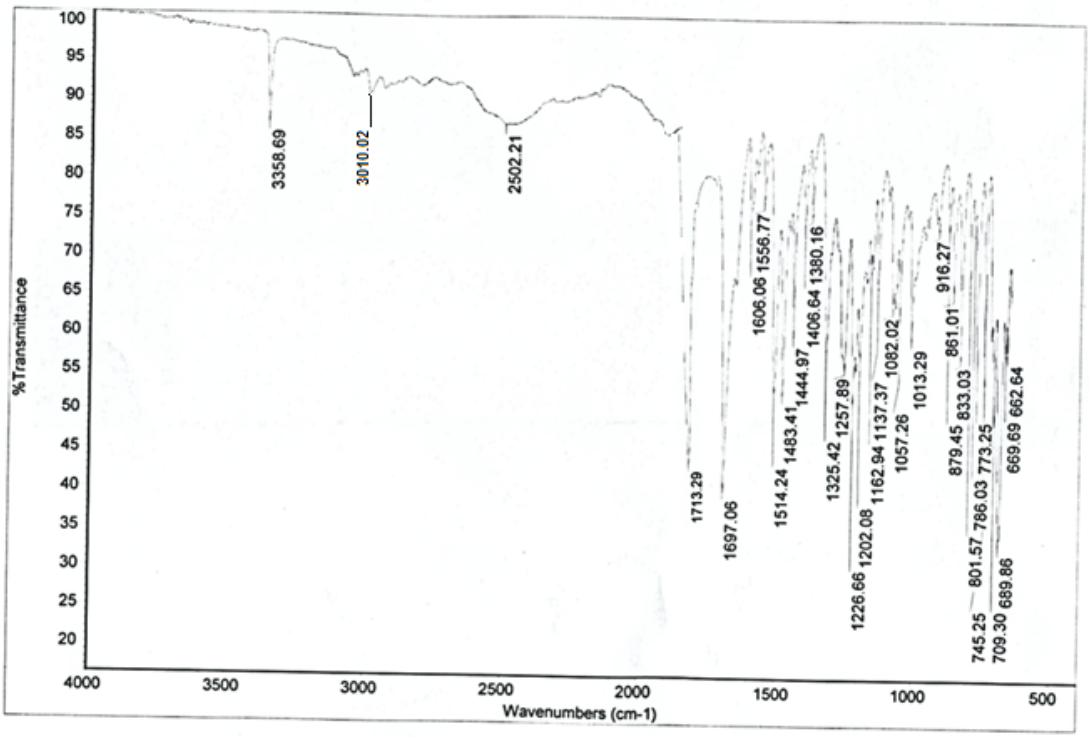

Figure S2. IR spectrum of Schiff base.

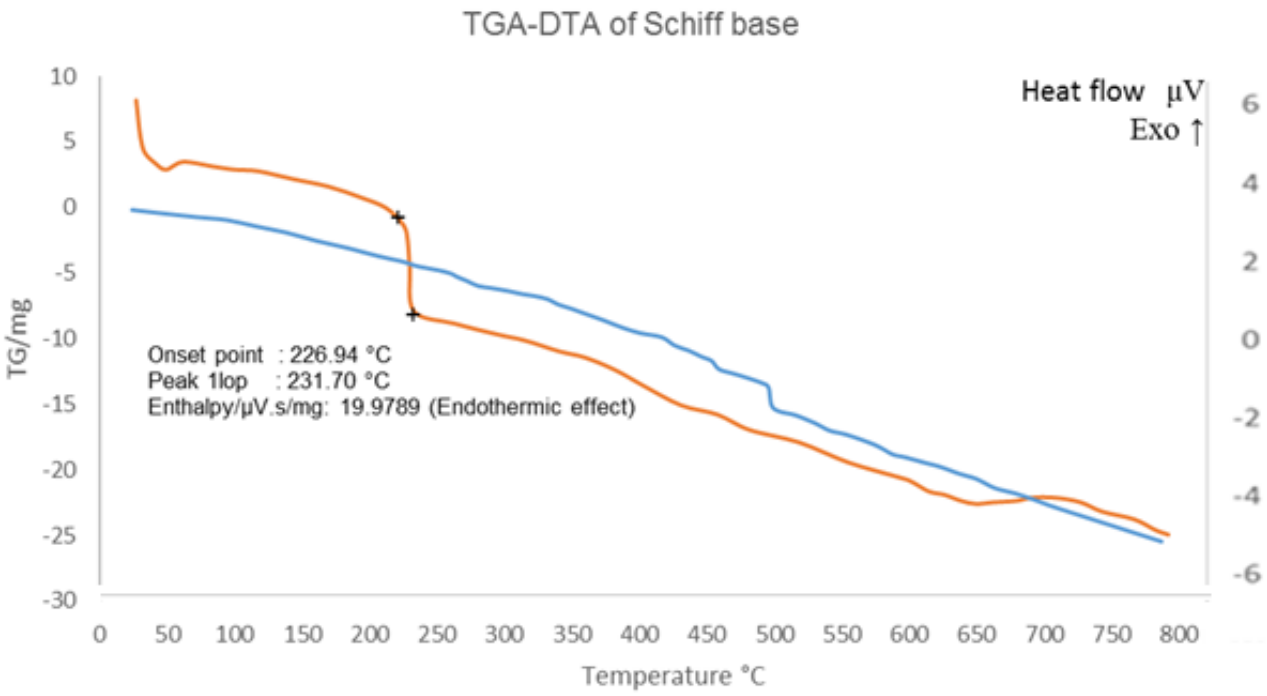

Figure S3. TGA-DTA of Schiff base (**1**).

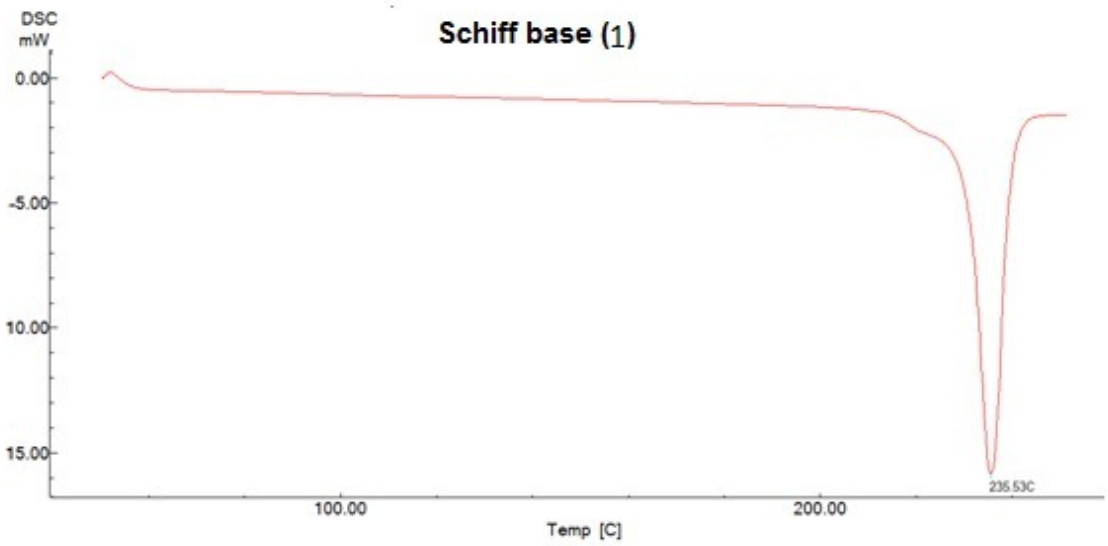

Figure S4. DSC of Schiff base.

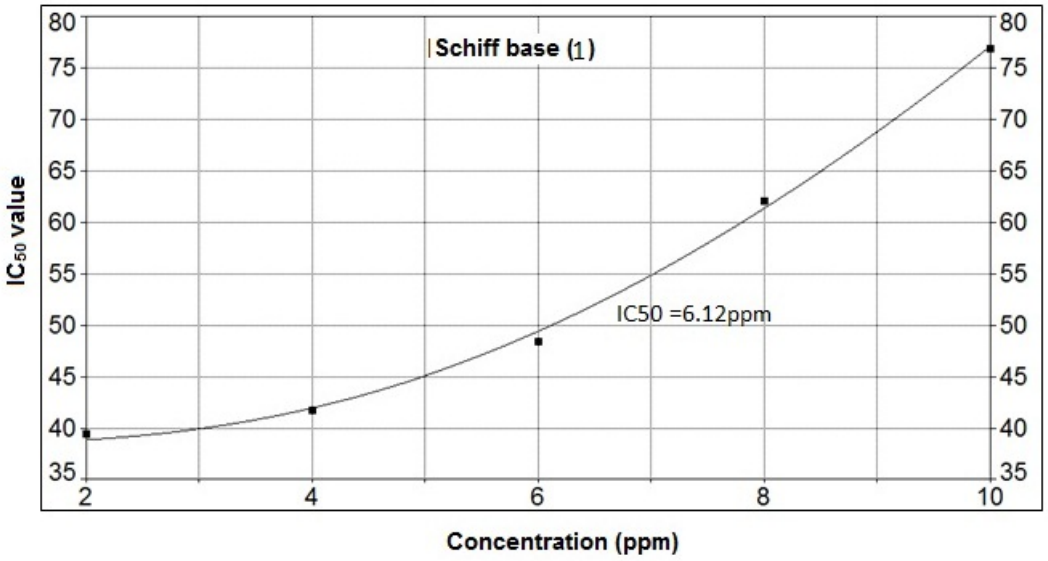

Figure S5. DPPH radical scavenging activity of Schiff base.

Table S1. TGA/DTA data of Schiff base.

Endothermic peak (DSC) (°C)	No. of stages	DTA peak temp (°C)	Thermogravimetry temp. range (°C)	Weight loss (%)	
				Found	Calc.
235.53	1	226	200–250	99	100

Table S2. Fluorescence data of Schiff base.

Compound	λex (nm)	λem (nm)	Stoke shift (nm)
$C_{22}H_{19}N_3O_3$	320	443	123

Table S3. DPPH radical scavenging activity of Schiff base.

DPPH radical scavenging activity (%)	
Compound	IC_{50} value (ppm)
Schiff base	6.12
Ketoprofen	92.85
Isoniazid	-

Table S4. Comparison of selected bond lengths (Å) and angles (°) for Schiff base using M06-2X /6-31G(d,p) and X-ray diffraction.

Bond length (Å)			Bond angle (°)		
	M06-2X	Exp		M06-2X	Exp
C1-C2	1.525	1.518	C2-C1-O26	112.6	111.5
C1-O26	1.326	1.305	C2-C1-O27	123.4	125.5
C1-O27	1.213	1.199	C1-C2-C3	110.6	112.9
C2-C3	1.528	1.481	C1-C2-C4	110.0	108.5
C2-C4	1.518	1.530	O26-C1-O27	124.0	122.9
C4-C5	1.399	1.372	C3-C2-C4	111.8	113.9
C4-C9	1.393	1.380	C2-C4-C5	120.5	121.6
C5-C6	1.390	1.388	C2-C4-C9	120.8	120.0
C6-C7	1.395	1.388	C5-C4-C9	118.8	118.5
C7-C8	1.395	1.379	C4-C5-C6	120.5	121.3
C8-C9	1.401	1.385	C4-C9-C8	121.2	121.2
C8-C10	1.499	1.497	C5-C6-C7	120.4	119.7
C10-C11	1.481	1.477	C6-C7-C8	119.8	119.3
C10-N23	1.288	1.284	C7-C8-C9	119.4	120.0
C11-C12	1.398	1.386	C7-C8-C10	121.6	119.7
C11-C16	1.402	1.386	C9-C8-C10	118.9	120.2
C12-C13	1.392	1.388	C8-C10-C11	120.1	120.0
C13-C14	1.390	1.367	C8-C10-N23	121.6	122.6
C14-C15	1.396	1.370	C11-C10-N23	118.2	117.4
C15-C16	1.387	1.379	C10-C11-C12	120.5	120.0
C17-C18	1.512	1.504	C10-C11-C16	120.3	121.3
C17-N24	1.369	1.348	C10-N23-N24	116.1	116.0
C18-C19	1.395	1.378	C12-C11-C16	119.2	118.6
C18-C22	1.393	1.382	C11-C12-C13	120.4	120.3
C19-C20	1.387	1.382	C11-C16-C15	120.2	120.7
C20-N25	1.336	1.326	C12-C13-C14	120.1	120.0
C21-C22	1.390	1.372	C13-C14-C15	119.7	120.4
C21-N25	1.340	1.325	C14-C15-C16	120.4	120.0
N23-N24	1.358	1.381	C18-C17-N24	112.2	114.5

Table S4. Continued.

Bond angle (°)		
	M06-2X	Exp
C17-C18-C19	123.7	125.1
C17-C18-C22	117.8	117.8
C17-N24-N23	122.6	120.7
C19-C18-C22	118.5	117.1
C18-C19-C20	118.5	119.1
C18-C22-21C	119.0	119.9
C19-C20-N25	123.2	123.7
C20-N25-C21	118.4	116.9
C22-C21-N25	122.4	123.3

Difference between DFT and experimental parameters are calculated by Exp – DFT; Diff = difference; Exp = experimental.

Table S5. Second-order perturbation theory analysis of selected Fock matrix of dimer using NBO method with M06-2X/6-311G(d,p) level theory.

Donor NBO (i)	Type	Acceptor NBO (j)	Type	E(2) kcal/mol a.u.	E(j) – E(i)	F(i,j)
C1-C2	σ	C2-C8	σ*	1.66	1.76	0.048
		C4-H6	σ*	1.69	1.47	0.045
		C8-C9	π*	1.71	0.78	0.035
		C8-C16	σ*	1.83	1.36	0.045
		O44-H45	σ*	3.63	1.62	0.069
C1-O44	σ	C2-C4	σ*	1.39	1.57	0.042
C1-O46	σ	C1-C2	σ*	1.06	1.66	0.038
C2-H3	σ	C1-O46	σ*	3.60	1.33	0.062
C8- C9	σ	C2-C8	σ*	1.97	1.24	0.044
C8-C9	π	C11-C13	π*	29.66	0.36	0.093
	π	C15-C16	π*	29.84	0.36	0.092
C11-C13	π	C8-C9	π*	27.68	0.37	0.091
	π	C15-C16	π*	32.67	0.35	0.097
C13-C15	σ	C11-H12	σ*	2.00	1.67	0.052
C15-C16	π	C8-C9	π*	29.11	0.38	0.094
	π	C11-C13	π*	27.82	0.37	0.090
C15-C18	σ	C11-C13	σ*	2.75	1.37	0.055
		C13-C15	σ*	2.48	1.38	0.052
		C15-C16	σ*	2.48	1.37	0.052
		C18-C19	σ*	1.88	1.27	0.044
		C18-N40	σ*	1.75	1.40	0.044
		C19-C28	σ*	1.39	2.39	0.052

Table S5. Continued.

Donor NBO (i)	Type	Acceptor NBO (j)	Type	E(2) kcal/mol a.u.	E(j) – E(i)	F(i,j)
C16-H17	σ	C8–C9	σ*	4.36	1.33	0.068
C18-H19	σ	C18-N40	σ*	2.19	1.40	0.050
		C19-C20	σ*	2.29	1.39	0.051
		C19-C28	σ*	2.61	1.39	0.054
C19-C20	π	C18-N40	π*	19.31	0.36	0.078
		C22-C24	π*	26.68	0.37	0.089
		C26-C28	π*	27.09	0.37	0.091
C22-C24	π	C19-C20	π*	29.06	0.36	0.092
		C26-C28	π*	27.38	0.37	0.091
C26-C28	π	C19-C20	π*	28.89	0.36	0.091
		C22-C24	π*	30.94	0.37	0.095
C31-C32	π	C30-O47	π*	16.54	0.38	0.073
		C34 -N43	π*	39.70	0.34	0.105
		C36-C38	π*	23.26	0.38	0.086
C32-N43	π	C36-C38	π*	33.88	0.43	0.108
C36-C38	π	C31-C32	π*	32.90	0.36	0.098
		C34- N43	π*	28.77	0.33	0.087
N40	LP (1)	C15-C18	σ*	13.05	0.97	0.101
N41	LP (1)	C18-N40	π*	28.41	0.40	0.099
	LP (1)	C30-O47	π*	76.66	0.39	0.157
N43	LP (1)	C32-C34	σ*	10.97	1.07	0.098
	LP (1)	C36-C38	σ*	10.30	1.09	0.096
	LP (1)	O91-H92	σ*	17.72	1.35	0.140
N90	LP (1)	O44-H45	σ*	17.72	1.35	0.140
O44	LP (1)	C1-O46	σ*	11.62	1.33	0.111
O44	LP (2)	C1-O46	π*	70.20	0.47	0.163

Table S6. Second-order perturbation theory analysis of selected Fock matrix of dimer using NBO method with M06-2X/6-311G(d,p) level theory and THF solvent.

Donor NBO (i)	Type	Acceptor NBO (j)	Type	E(2) kcal/mol a.u.	E(j) – E(i)	F(i,j)
C1-C2	σ	C2-C8	σ*	1.22	1.17	0.034
C1-C2	σ	C4-H6	σ*	1.79	1.25	0.042
C1-C2	σ	C8-C9	π*	1.59	0.77	0.034
C1-C2	σ	C8-C16	σ*	1.87	1.35	0.045
C1-O44	σ	C2-C4	σ*	1.18	1.49	0.038
C1-O46	σ	C1-C2	σ*	0.94	1.63	0.036
C2-H3	σ	C1-O46	σ*	3.65	1.24	0.060
C2-H3	σ	C8-C9	σ*	4.81	1.19	0.068
C2-C4	σ	C1-O44	σ*	3.18	1.15	0.055
C8- C9	σ	C2-C8	σ*	2.26	1.24	0.047
C8- C9	σ	C8-C16	σ*	4.13	1.41	0.068
C8-C9	π	C11-C13	π*	29.65	0.35	0.092
C8-C9	π	C15-C16	π*	31.24	0.34	0.092
C11-C13	π	C8-C9	π*	29.10	0.36	0.091
C11-C13	π	C15-C16	π*	31.27	0.34	0.093
C13-C15	σ	C11-H12	σ*	2.27	1.35	0.050
C15-C16	π	C8-C9	π*	28.44	0.36	0.091
C15-C16	π	C11-C13	π*	27.33	0.36	0.089
C15-C18	σ	C8-C16	σ*	2.83	1.37	0.056
C15-C18	σ	C11-C13	σ*	2.37	1.37	0.051
C15-C18	σ	C13-C15	σ*	2.71	1.36	0.054
C15-C18	σ	C15-C16	σ*	2.36	1.35	0.050
C15-C18	σ	C18-C19	σ*	1.88	1.26	0.044
C15-C18	σ	C18-N40	σ*	1.67	1.39	0.043
C15-C18	σ	C19-C28	σ*	2.39	1.37	0.051
C16-H17	σ	C8-C9	σ*	4.52	1.22	0.066
C16-H17	σ	C13-C15	σ*	4.58	1.22	0.067
C18-H19	σ	C18-N40	σ*	2.11	1.39	0.049
C18-H19	σ	C19-C20	σ*	2.42	1.37	0.052
C18-H19	σ	C19-C28	σ*	2.56	1.37	0.053
C18-H19	σ	C20-C22	σ*	2.17	1.38	0.049
C18-H19	σ	N40-N41	σ*	5.42	1.18	0.072
C19-C20	π	C18-N40	π*	20.02	0.35	0.078
C19-C20	π	C22-C24	π*	26.82	0.36	0.089
C19-C20	π	C26-C28	π*	26.28	0.36	0.089

Table S6. Continued.

Donor NBO (i)	Type	Acceptor NBO (j)	Type	E(2) kcal/mol a.u.	E(j) – E(i)	F(i,j)
C22-C24	π	C19-C20	π*	30.06	0.35	0.093
C22-C24	π	C26-C28	π*	26.60	0.36	0.089
C26-C28	π	C19-C20	π*	27.72	0.35	0.089
C26-C28	π	C22-C24	π*	28.80	0.36	0.091
C31-C38	π	C30-O47	π*	17.29	0.37	0.073
C31-C38	π	C32-C34	π*	24.86	0.36	0.086
C31-C38	π	C36-N43	π*	41.93	0.33	0.105
C32-N43	π	C31-C38	π*	31.54	0.36	0.097
C32-N43	π	C36-C38	π*	26.17	0.33	0.084
C36-C43	π	C31-C38	π*	17.51	0.42	0.078
C36-C43	π	C32-C34	π*	35.14	0.42	0.109
N40	LP (1)	C15-C18	σ*	12.56	0.96	0.099
N41	LP (1)	C18-N40	π*	31.66	0.39	0.103
N41	LP (1)	C30-O47	π*	72.71	0.38	0.151
N43	LP (1)	C32-C34	σ*	10.97	1.07	0.098
N43	LP (1)	C36-C38	σ*	10.30	1.09	0.096
O44	LP (1)	C1-O46	σ*	11.05	1.32	0.108
O44	LP (2)	C1-O46	π*	70.04	0.44	0.157
O46	LP (2)	C1-O44	σ*	34.23	0.81	0.151

Table S7. Molecular frontier orbital energy, ionization potential (*IP*), electron affinity (*EA*), electronegativity (*X*), chemical potential (μ), global hardness (η), global softness (*S*), and global electrophilicity (ω).

MO(s)	Energy	ΔE	*IP*	*EA*	*X*	μ	η	*S*	ω
HOMO	–0.2780	0.2330	0.2780	0.0449	0.1615	–0.1615	0.1165	4.2902	0.1119
LUMO	–0.04498								
HOMO-1	–0.2781	0.2331	0.2781	0.0449	0.1615	–0.1615	0.1165	4.2886	0.1119
LUMO+1	–0.0449								

$\Delta E = E_{LUMO} - E_{HOMO}$; units in Hartree (a.u.)

Frontier molecular orbitals (FMOs).

Equations for global reactivity descriptors:

$$IP = -E_{HOMO}$$

$$EA = -E_{LUMO}$$

$$X = \frac{[IP + EA]}{2} = -\frac{[E_{LUMO} + E_{HOMO}]}{2}$$

$$\eta = \frac{[IP - EA]}{2} = -\frac{[E_{\mathrm{LUMO}} - E_{\mathrm{HOMO}}]}{2}$$

$$\mu = \frac{E_{\mathrm{HOMO}} + E_{\mathrm{LUMO}}}{2}$$

$$\sigma = \frac{1}{2\eta}$$

$$\omega = \frac{\mu^2}{2\eta}$$

Here, *IP* is ionization potential (a.u.), *EA* is electron affinity (a.u.), (X) is electronegativity, (η) is chemical hardness, (μ) is chemical potential, (σ) is global softness, and (ω) is electrophilicity index.